MIT.3 Integration of SASS Ku-Band Imagery and AVHRR Imagery for Historical Tropical Forest Inventory

P.J. Hardin[1], D.G. Long[2]

Brigham Young University, 690 SWKT, Provo, Utah 84602

[1]Department of Geography, [2]Department of Electrical and Computer Engineering

Introduction

Currently there is an extended international effort to inventory and monitor the global rain forests. Because of persistent cloud cover in the tropical rain forest regions, active microwave imagery such as ERS-1 SAR is preferred over high-resolution visible and near infrared spaceborne sensors. Nevertheless, because many rain forests cover such vast regions, AVHRR imagery and its derivative vegetation indices are frequently utilized for medium or low-resolution monitoring where comprehensive high-resolution imaging would create unmanageable data volumes, or would be cost prohibitive. However, AVHRR suffers from the same cloud cover problem as its higher resolution counterparts in humid regions of the world. Clearly an active microwave instrument with a 1-12km resolution would be desirable in providing global coverage of tropical forest regions under these conditions, but no active microwave instrument designed to provide land coverage at this resolution has never flown -- neither are any planned for the future.

The research described below reports initial progress to integrate and compare AVHRR vegetation index images with historical SASS imagery reconstructed to comparable resolutions. The study area incorporates several states in *Brasil*, and includes tropical forest, savanna, grassland, and secondary vegetation formations. First, we will briefly describe the SASS data source and reconstruction process. We will next describe the AVHRR data source and processing required to integrate the vegetation index set with the reconstructed SASS data. We then proceed to compare the vegetation index values and backscatter response of sixteen different vegetation formations found in the study area. Finally, we offer conclusions and directions for further research.

SASS and the Image Reconstruction

Spaceborne scatterometers transmit microwave pulses to the ocean surface and measure backscattered power received at the instrument, allowing estimation of the normalized radar cross section (σ^0) of the surface. From each illuminated location on the earth, the total power received by a radar is the sum of the power backscattered by the target, noise from the frequency-specific natural emissivity of the earth-atmosphere system, and noise from the instrument itself. Once noise is subtracted from the total received power, σ^0 can then be calculated using the basic radar equation.

Although primarily designed for oceanic wind studies, data from the Seasat-A Scatterometer (SASS) was also collected over global regions of ice and land during the ill-fated three month flight of Seasat-A between June 27 and October 10, 1978. Although the native resolution of SASS is approximately 50 km, Long *et al.* (1993) have developed techniques to reconstruct medium-scale imagery with pixel resolutions between 4 and 12 kilometers over land from these lower-resolution scatterometer measurements acquired at a variety of incidence and azimuth angles. Assuming no azimuthal modulation, we determined that, over the narrow incidence angle range between 23° and 55°, the incidence angle dependence of σ^o for the study region could be described by $10\log_{10}\sigma^o(\theta) = A + B(\theta - 40^o)$, where A and B are independent of the incidence angle θ and dependent on the target character, and where β is dependent on θ. In the process of reconstruction, images of A and B are created which are used in lieu of a σ^o image. Because of the diversity of measurement incidence angles used by wind scatterometers, the A and B coefficients of this model are more useful in application than direct σ^0 measurements. Generally speaking, A can be considered the "incidence angle-normalized σ^0.

The key to achieving high resolution by signal processing is overlap in the SASS σ^o measurements. However, the SASS σ^o measurements made by a single antenna on a single beam during one orbit had no overlap, and the forward and aft beam measurements overlapped only a small amount. Furthermore, when this lack of overlap is combined with the problem of small gaps in the surface coverage for a single orbit, the result is insufficient data to attempt the resolution improvement scheme with data from a single SASS pass. However, due to precession in the spacecraft orbit, a point on the earth's surface was observed from the same beam with slightly different azimuth and incidence angles about once every three days. Data was also acquired by the instrument on both ascending and descending orbital nodes. The resulting set of criss-crossing measurement swaths in a single orbit combined from several orbits provides ample overlap to facilitate accurate estimation of A and B over equatorial regions.

Limitations of Reconstructed SASS Imagery

For the interpretability of the reconstructed image to be maximized, the target should reasonably satisfy several criteria. Obviously, we assume that the linear model cited above adequately describes the incidence angle dependence of σ^o over the range of incidence angles used. Furthermore, the value of σ^o of the same location should not vary from orbit to orbit. In practical terms, this implies that the landscape should not change during the acquisition period. More specifically, the value of σ^o should not vary according to the time of day, neither should it vary from day to day for the period of acquisition. The dependence of σ^o on the azimuth angle should also be small or known. The interested reader is invited to review Birrer *et al.* (1982) for a discussion of how these assumptions are satisfied in this study area.

One other prerequisite for successful reconstruction deserves special mention, since it is a critical

factor in passive optical and near-infrared remote sensing of equatorial regions. Thick clouds and heavy rainfall should not persist over the same location during the acquisition period. It is common knowledge that rainfall can attenuate backscatter at 14.6 Ghz frequencies. In a preliminary analysis of Amazon region SASS data, Birrer *et al.* (1982) utilized GOES imagery to remove all the SASS measurements which showed significant cloud cover. The procedure was quickly deemed unnecessary and abandoned, as "few measurements should have been corrupted" due to the dry season acquisition. Our own empirical evidence supports these conclusions.

AVHRR and the Global Vegetation Index Products

Early work by Tarpley *et al.* (1984) and others demonstrated that vegetation indices derived from NOAA polar orbiter sensors were extremely useful for monitoring vegetation on a continental scale. The Global Vegetation Index (GVI) product produced by NOAA is an extensive collection of weekly vegetation index images available in a variety of map projections. These weekly images are composites derived from daily Advanced Very High Resolution (AVHRR) global area coverage (GAC) data.

Several vegetation indices are reported in the literature, however two of the most common are the simple Green/Red and Infrared / Red ratios derived from visible and infrared instruments. The greenness vegetation index, one of several GVI measures available, is a ratio of AVHRR Channel 2 (0.73 - 1.10 μm) to Channel 1 (0.58 - 0.68 μm). This ratio is designated in this paper as *IR/R*. However, the normalized difference vegetation index (*NDVI*), defined as (Channel 2 - Channel 1) / (Channel 2 + Channel 1) is preferred to *IR/R* because it compensates to a certain extent for viewing aspect, terrain slope, and changes in illumination (Kidwell, 1990). Both *IR/R* and *NDVI* indices were utilized in this project.

Limitations of the First Generation GVI products

A processing overview of the first and second generation GVI products can be found in Kidwell (1990). While NOAA has been creating successively better GVI products, the first generation products used in this study were experimental, and have a few inherent limitations for equatorial studies of vegetation. First, the imagery is cast in two hemispheric polar stereographic projections with the resolution changing from 13 kilometers at the equator to 26 kilometers at the poles. This projection is inconvenient for equatorial studies, since the area of interest is split between the two hemispheres in the projection. This makes visualization, interpretation and registration difficult. Secondly, the processing methodology to combine the daily data into weekly data changed three times over a several month period in 1982. This was precisely the period of interest in this study. The reader is invited to review Kidwell (1990) for a discussion of these processing changes. In the examination described below, these processing differences become noise. Other limitations in the GVI products, along with suggestions for their correction is summarized in Tateishi and Kajiwara (1992) and Kaufman *et al.* (1992).

An Experiment in Integration and Comparison

The reconstructed SASS imagery is a composite formed from data collected over *Brasil* from July to early October, 1978. To integrate the GVI products successfully with the SASS imagery and make the imagery comparable, seasonal GVI composites were constructed for the same seasonal period, albeit in 1982. The integration procedure is outlined in Figure 1.

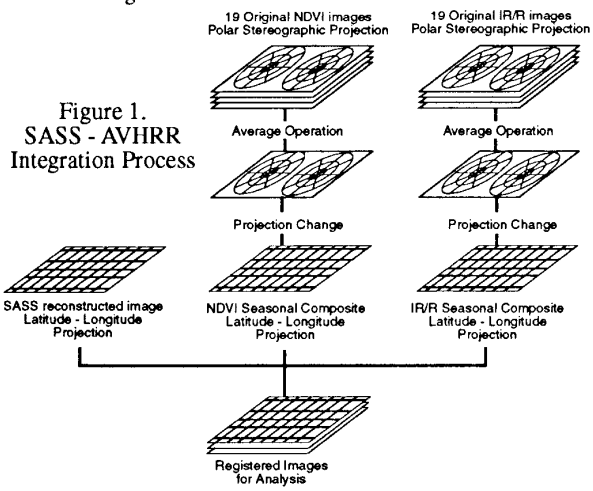

Figure 1.
SASS - AVHRR
Integration Process

Nineteen GVI image data sets, corresponding to the weeks between Monday, May 31, 1982 and Sunday, October 10, 1982 were averaged on a pixel-by-pixel basis to produce the required seasonal GVI composites -- one composite representing the seasonal *NDVI*, and the other representing the seasonal *IR/R* average. These composites, cast on a polar-stereographic projection, were next recast to the identical latitude/longitude graticule as the SASS image to achieve precise registration of the three data sets. Since the pixel size of the GVI data set in this region (approximately 14 km) was much coarser than the SASS data set (approximately 5 km), nearest neighbor interpolation was utilized to fill the 5km pixels in the final GVI images.

A simple procedure was devised to compare the GVI imagery to the SASS imagery for discriminating between broad vegetation classes within *Brasil*. Using the 1:5,000,000 scale *Mapa de Vegetacao do Brasil*, several polygons were delimited for 16 different Brazilian vegetation formations. Realizing the limitations of the map source material, the inexact nature of cartographic classification, unavoidable generalizations, and the difficulties in drawing exact boundaries for vegetation classes which likely blend in transition zones, the polygons were delimited only for the larger mapped areas of vegetation. Once these polygons were digitized, the corresponding pixels were extracted from the SASS *A*, *IR/R* and *NDVI* images and saved for further analysis.

The analysis consisted of two parts. In the first part of the analysis, the goal was to explore the relationship between the GVI and *A* values for each vegetation formation. Since backscatter response of tropical vegetation at Ku-band frequencies is almost entirely unstudied, it was hoped that this examination would provide insight concerning scattering mechanisms.

In the second part, some exploratory discrimination was performed to determined whether the combined data sets would be useful for land cover mapping of the vegetation formations. In the discrimination tests described below, only one half of the pixels for each of the 16 formations were used for training. The remaining half were reserved for testing the

discrimination. The fundamental approach used in the exploratory discriminant analysis was to continually regroup the original 16 categories into a much smaller set until the classification accuracy produced by discriminant functions reached an acceptable level. An effort was made to maintain logically consistent groupings. The quality of the supervised classification was assessed by calculating both an overall Cohen's kappa (κ) measure. Various combinations of *A, IR/R* and *NDVI* were tried in the discrimination experiments in order to find the optimum combination for classification.

Results

A summary of the 16 vegetation classes is given in Table 1. The table is sorted by *A* value. As the table shows, the ombrophilous forest types had the highest *A* values, followed in general by the savanna and seasonal forests. The grassland and open parkland savannas (S, Sa) had the lowest *A* response. The *IR/R* and *NDVI* class mean values showed the same basic trend. As shown in Figures 2 and 3, there is a moderate linear relationship between the sixteen mean class *A* and *IR/R* values (r=0.81), and between the sixteen mean class *A* and *NDVI* values (r= 0.76). Steppe and open parkland steppe are significant outliers, particularly in the *NDVI* graph.

While the correlation may be high when the mean class responses are compared, on a pixel-by-pixel basis the correlation between *A* and *IR/R* is only 0.173, and the relationship between *A* and NDVI is 0.172. These low correlations are an artifact we attribute to the different original resolutions of the two images.

As mentioned above, initial attempts were made to classify the 16 formations. Depending on the confusion between them, the groups were then combined. Table 2 lists the final 4 group classification. The groups included ombrophilous forest, steppe, seasonal forest, and savanna. Mixed classes such as SN, EN, LO, ON, and PA were excluded from the 4-class aggregation. As shown in Table 3, all possible combinations of *A, NDVI*, and *IR/R* were used in the discrimination experiments. When we attempted to discriminate between all 16 classes, use of all three variables produced the highest accuracy (kappa = 0.51). In the four group experiment, very high accuracies were achieved when *A* was combined with one of the vegetation indices. Addition of the remaining vegetation index was insignificant.

Conclusions

Given the success of this discrimination experiment, further research into combining SASS and AVHRR data may bring substantial payoffs. In such a project, much of the confusion in a purely optical-infrared or backscatter-based classification could be removed by incorporating the other image type and other ancillary data sources. It may then be possible to extend the procedure using the global SASS and AVHRR data sets to all the equatorial regions of the world in order to estimate and map the historical extent of the global subtropical forests into broad categories. With the launch of ADEOS in 1995 and the high resolution ground processing of NSCAT imagery using similar techniques, the potential may exist to assess change in the subtropical forest character and extent over the seventeen year interval at identical spatial resolutions and frequencies. Unlike the SASS data which covered only three months, NSCAT and AVHRR coverage of the equatorial and savanna regions for the entire year would also allow change in backscatter, *NDVI*, and *IR/R* through the seasons to be used as a discriminator for more accurate vegetation mapping.

However, the potential for utilizing SASS-AVHRR image sets goes beyond land cover mapping or monitoring. The existence of several vegetation class gradations within and between the formations, along with the strong correlation between the backscatter and NDVI class values indicates the strong possibility of obtaining critical quantitative information about subtropical vegetation community character from these integrated data sets. While the correlation between the data

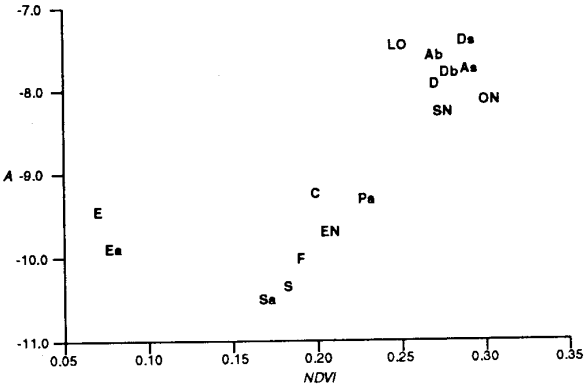

Figure 2.

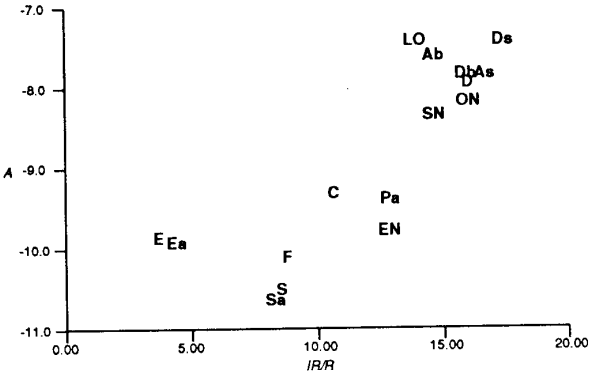

Figure 3.

sets leads us to believe that 14.6 Ghz backscatter in equatorial areas is a function of canopy density, it is possible these backscatter coefficients also change in response to canopy vigor, canopy moisture, another canopy structural characteristic, or more complex quantitative variables.

Land scatterometry, combined with medium resolution optical and infrared imagery can potentially play an important role in tropical studies requiring fusion of data from sensors of moderate spatial resolutions. Furthermore, using higher resolution SAR, visible, thermal, and infrared imagery of carefully selected field sites as primary data sources, it may be possible to use high resolution reconstructed scatterometer imagery and AVHRR imagery together in order to extend derived estimates of biomass, canopy structure, moisture content, or transpiration rates over large regions.

References

Birrer, I.J., E.M. Bracalente, G.J. Dome, J. Sweet, and G. Berthold, 1982. σ^0 Signature of the Amazon Rainforest Obtained from the Seasat Scatterometer. *IEEE Transactions on Geoscience and Remote Sensing*, GE-20, No. 1, pp. 11-17.

Kaufman, Y.J., D. Tanre', B.N. Holben, B. Markham, and A. Gitelson, 1992. Atmospheric Effects on the NDVI -- Strategies for its Removal. *IGARSS '92*, pp. 1238-1241.

Kidwell, K.B., 1990. *Global Vegetation Index User's Guide.* U.S. Department of Commerce, National Oceanic and Atmospheric Administration.

Long, D.G., P.J. Hardin, and P.T. Whiting, 1993. High Resolution Imaging of Land/Ice using Spaceborne Scatterometry Part I: The Imaging Technique. *IEEE Transactions on Geoscience and Remote Sensing.* (In press).

Tarpley, J.D., S.R. Schneider, and R.L. Money, 1984. Global Vegetation Indices from the NOAA-7 Meteorological Satellite. *Journal of Climate and Applied Meteorology*, 23:491-494.

Tateishi, R. and K. Kajiwara, 1992. Global Land Cover Monitoring by NOAA GVI Data. *IGARSS '92*, pp. 1637-1639.

Class Name	Symbol	*n*	*A* (db)	*IR/R*	*NDVI*
Dense Submontane Ombrophilous Forest	Ds	6355	-7.39	17.31	0.289
Extremely Moist Tropical Ombrophilous Lowland Swamp Forest	LO	1305	-7.45	14.19	0.251
Open Ombrophilous Forest: *Terras Baixas*	Ab	1679	-7.57	14.85	0.274
Open Submontane Ombrophilous Forest	As	1594	-7.77	16.13	0.288
Dense Ombrophilous Forest: *Terras Baixas*	Db	3412	-7.80	15.82	0.281
Dense Ombrophilous Forest	D	1040	-7.94	15.94	0.267
Ombrophilous Forest -- Seasonal Forest	ON	1352	-8.12	15.99	0.305
Savanna -- Seasonal Forest	SN	403	-8.29	14.80	0.275
Seasonal Deciduous Forest	C	960	-9.26	10.51	0.201
Riparian Forest and Related Formations	Pa	298	-9.31	12.89	0.230
Steppe	E	786	-9.48	3.52	0.077
Seasonal Forest Steppe	EN	343	-9.70	12.78	0.214
Open Parkland Steppe	Ea	869	-9.89	4.30	0.086
Semideciduous Seasonal Forest	F	3773	-9.99	8.96	0.193
Savanna	S	1061	-10.38	8.74	0.183
Open Parkland Savanna	Sa	1290	-10.51	8.30	0.172
Summary		26520	-8.46	13.42	0.243

Table 1.

Aggregate Class Name	Original Classes	*A*		*IR/R*		*NDVI*	
		mean	std dev	mean	std dev	mean	std dev
Ombrophilous Forest	D,Db,Ds,Ab,As	-7.59	0.381	16.42	1.69	0.283	0.0179
Steppe	E,Ea	-9.70	0.635	3.93	1.70	0.082	0.0274
Seasonal Forest	F,C	-9.84	0.781	9.28	2.13	0.195	0.0341
Savanna	S,Sa	-10.45	0.611	8.50	1.52	0.177	0.0279
Summary		-8.51	1.290	13.22	4.61	0.240	0.0661

Table 2.

Discrimination Variables Used	16-Class Experiment		4-Class Experiment	
	Kappa	Classifier	Kappa	Classifier
IR/R alone	0.351	QDP	0.740	LDF
NDVI alone	0.299	QDP	0.746	LDF
A alone	0.312	QDP	0.674	QDP
IR/R and *NDVI*	0.437	QDP	0.772	LDF
A and *IR/R*	0.461	QDP	0.791	QDP
A and *NDVI*	0.464	QDP	0.791	QDP
A, *IR/R*, and *NDVI*	0.505	QDP	0.800	QDP

Table 3.

QDP = Quadratic Discriminant Function

LDF = Linear Discriminant Function